International Journal of Theoretical Physics, Vol. 42, No. 2, February 2003 (© 2003)

Digital Studies and Perspectives for N-Body Modelling in Physics

Donald Greenspan[1]

Received August 22, 2001

In 1977, Richard Feynman, in an invited lecture at the national APS meeting, stated unequivocally that quantum mechanical principles placed few important restrictions on how a stable atom can be held in place, and, indeed, a stable atom on the whole has a comparatively definite position fixed by its comparatively massive nucleus. In this spirit, N-body problems are studied using molecules and classical molecular potentials and also using collections of molecules, called particles, with related potentials derived through conservation of mass and energy. Detailed applications include primary vortex flow and turbulent flow for both water vapor and air, soliton collision, and the motion of a top on a smooth surface. Other applications, like microdrop collision, stress of a slotted copper plate, contact angle of adhesion, cellular self-reorganiztion, the bounce of an elastic ball, and elastic snap-through are mentioned and referenced appropriately. Lastly, numerical methodology is developed which preserves the physics of special relativity and is applied to simulate a relativistic oscillator.

KEY WORDS: N-body; molecules; particles; conservation laws; special relativity.

1. PHYSICAL, MATHEMATICAL, AND COMPUTATIONAL PRELIMINARIES

1.1. N-Body Problems

Our concern throughout will be with the N-body problem. The N-body problem is described in complete generality as follows. In cgs units and for $i = 1,2,\ldots,N$, let P_i of mass m_i be at $\vec{r}_i = (x_i, y_i, z_i)$, have velocity $\vec{v}_i = (v_{i,x}, v_{i,y}, v_{i,z})$, and have acceleration $\vec{a}_i = (a_{i,x}, a_{i,y}, a_{i,z})$ at time $t \geq 0$. Let the positive distance between P_i and P_j, $i \neq j$, be $r_{ij} = r_{ji} \neq 0$. Let the force on P_i due to P_j be $\vec{F}_{ij} = \vec{F}_{ij}(r_{ij})$, so that the force depends only on the distance between P_i and P_j. Also, assume that the force $\vec{F}_{ji}$ on P_j due to P_i satisfies $\vec{F}_{ji} = -\vec{F}_{ij}$. Then, given the intial positions and velocities of all the P_i, $i = 1,2,3,\ldots,N$, the general N-body problem is to determine the motion of the system if each P_i interacts with all the other P_j's in the system.

[1] Mathematics Department, University of Texas at Arlington, Arlington, Texas 76019.

0020-7748/03/0200-0249/0 © 2003 Plenum Publishing Corporation

1.2. Classical Molecular Forces

Classical molecular forces behave, in general, as follows (Feynam *et al.*, 1963):

- when two close molecules are pulled apart, they attract;
- when pushed together, they repel; and
- repulsion is of a greater order of magnitude than is attraction.

The most important exception to this general behavior is the basic fluid of living matter, that is, liquid water, the primary reason being that close liquid water molecules exhibit hydrogen bonding. It should be noted however that these bonds are not strong and that the average number of molecules, or the cluster size, which exhibit such bonds decreases with temperature and pressure. Also, it is not known if such bonds exist if a flow is turbulent.

There are a variety of classical molecular potentials for the interactions of molecules and from these classical molecular force formulas can be derived (Hirschfelder *et al.*, 1967). There are, for example, Buckingham, Lennard–Jones, Morse, Slater–Kirkwood, Stockmayer, Sutherland, and Yntema–Schneider potentials. The potential which has received the most attention is the Lennard–Jones potential, that is,

$$\phi(r_{ij}) = 4\epsilon \left[\frac{\sigma^{12}}{r_{ij}^{12}} - \frac{\sigma^{6}}{r_{ij}^{6}} \right] \text{erg}, \tag{1}$$

in which r_{ij} is measured in Angstroms. In (1), the term with exponents 12 is the repulsion term and the term with exponents 6 is the attraction term. As r_{ij} goes to zero, the resulting motion is volatile.

For example, an approximate Lennard–Jones potential for water vapor molecules is

$$\phi(r_{ij}) = 1.9646 \cdot 10^{-13} \left[\frac{2.725^{12}}{r_{ij}^{12}} - \frac{2.725^{6}}{r_{ij}^{6}} \right] \text{erg}, \tag{2}$$

in which, with respect to (1), $4\epsilon = 1.9646 \cdot 10^{-13}$ and $\sigma = 2.725$. The force $\vec{F}_{ij}$ exerted on P_i by P_j is then

$$\vec{F}_{ij} = 1.9646 \cdot 10^{-5} \left[\frac{12 \cdot 2.725^{12}}{r_{ij}^{13}} - \frac{6 \cdot 2.725^{6}}{r_{ij}^{7}} \right] \frac{\vec{r}_{ji}}{r_{ij}} \text{dynes}. \tag{3}$$

Note that $F_{ij} = \|\vec{F}_{ij}\| = 0$ implies that $r_{ij} = 3.06$ Å, which is the equilibrium distance, with repulsion prevailing if $r_{ij} < 3.06$ and attraction prevailing if $r_{ij} > 3.06$. Note also that in a regular triangle with edge $r_{ij} = 3.06$ Å, the altitude is 2.65 Å.

1.3. Equations of Motion for Water Vapor Molecules

In molecular mechanics we simulate the motion of a system of molecules using classical molecular potentials and Newtonian mechanics. Thus the motion for a single water vapor molecule P_i acted on by a single water vapor molecule P_j, $i \neq j$, is then

$$m_i \vec{a}_i = 1.9646 \cdot 10^{-5} \left[\frac{12(2.725^{12})}{r_{ij}^{13}} - \frac{6 \cdot 2.725^6}{r_{ij}^7} \right] \frac{\vec{r}_{ij}}{r_{ij}}. \tag{4}$$

Since the mass of a water molecule is $30.103 \cdot 10^{-24}$ gr, the latter equation is equivalent to

$$\vec{a}_i = 160.33 \cdot 10^{19} \left[\frac{818.90}{r_{ij}^{13}} - \frac{1}{r_{ij}^7} \right] \frac{\vec{r}_{ji}}{r_{ij}} \left(\frac{\text{cm}}{\text{s}^2} \right). \tag{5}$$

Recasting the latter equation in $\text{Å}/(\text{ps}^2)$ yields

$$\vec{a}_i = 160,330 \left[\frac{818.90}{r_{ij}^{13}} - \frac{1}{r_{ij}^7} \right] \frac{\vec{r}_{ji}}{r_{ij}} \left(\frac{\text{Å}}{\text{ps}^2} \right). \tag{6}$$

On the molecular level, however, the effective force on P_i is local, that is, it is determined only by close molecules. But, because of our interest in turbulence, in which the forces are so great that attraction is of lesser importance, we will take local to mean the solution of the equation

$$\frac{dF_{ij}}{dr_{ij}} = 0. \tag{7}$$

The solution to this equation yields $r_{ij} = 3.39$ Å. Thus, for $r_{ij} \geq D = 3.39$ Å, we choose $\vec{F}_{ij} = \vec{0}$. Note that it is more common to choose $D = 3\sigma$.

From (5), then, the dynamical equation for water molecule P_i will be

$$\frac{d^2\vec{r}_i}{dt^2} = 160,330 \sum_{\substack{j \\ j \neq i}} \left[\frac{818.90}{r_{ij}^{13}} - \frac{1}{r_{ij}^7} \right] \frac{\vec{r}_{ji}}{r_{ij}}, \qquad r_{ij} < D. \tag{8}$$

The equations of motion for a system of water molecules are then

$$\frac{d^2\vec{r}_i}{dt^2} = 160,330 \sum_{\substack{j \\ j \neq i}} \left[\frac{818.90}{r_{ij}^{13}} - \frac{1}{r_{ij}^7} \right] \frac{\vec{r}_{ji}}{r_{ij}}, \qquad i = 1, 2, 3, \ldots N, \quad r_{ij} < D. \tag{9}$$

Note that on the molecular level gravity can be neglected since 980 $\text{cm/s}^2 = (980)10^{-16}$ Å/ps^2. Note also that in simulating the motion of a system of N molecules, nonlinear Eq. (9) forewarns us that we will have to solve large systems

of nonlinear, second-order, ordinary differential equations ($2N$ in two dimensions and $3N$ in three dimensions), and that these will have to be solved numerically. The method to be used is based on the leapfrog formulas.

1.4. The Leapfrog Formulas

Classical molecular force formulas require small time steps in any numerical simulation to yield physically correct results for the effect of repulsion, which is unbounded when the distance between the molecules is close to zero. Because we are restricted physically to small time steps and because the number of equations is usually exceptionally large, Runge-Kutta and Taylor expansion methods, for example, prove to be unwieldy for related problems. Hence, in this section we will describe a simplistic, efficient, but low-order method, called the *leapfrog* method, for molecular mechanics simulations and it is described as follows (Greenspan, 1997).

Choose a positive time step Δt and let $t_k = k\Delta t$, $k = 0,1,2, \ldots$. For $i = 1,2,3, \ldots, N$, let P_i have mass m_i and at t_k let it be at

$$\vec{r}_{ik} = (x_{ik}, y_{i,k}, z_{i,k}),$$

have velocity

$$\vec{v}_{i,k} = (v_{i,k,x}, v_{i,k,y}, v_{i,k,z}),$$

and have acceleration

$$\vec{a}_{i,k} = (a_{i,k,x}, a_{i,k,y}, a_{i,k,z}).$$

The leapfrog formulas, which relate position, velocity, and acceleration, are

$$\frac{\vec{v}_{i,\frac{1}{2}} - \vec{v}_{i,0}}{\frac{1}{2}\Delta t} = \vec{a}_{i,0}, \quad \text{(starter)}, \tag{10}$$

$$\frac{\vec{v}_{i,k+\frac{1}{2}} - \vec{v}_{i,k-\frac{1}{2}}}{\Delta t} = \vec{a}_{i,k}, \qquad k = 1, 2, 3, \ldots, \tag{11}$$

$$\frac{\vec{r}_{i,k+1} - \vec{r}_{i,k}}{\Delta t} = \vec{v}_{i,k+\frac{1}{2}}, \qquad k = 0, 1, 2, 3, \ldots, \tag{12}$$

or, explicitly,

$$\vec{v}_{i,\frac{1}{2}} = \vec{v}_{i,0} + \frac{1}{2}(\Delta t)\vec{a}_{i,0} \quad \text{(starter)}, \tag{13}$$

$$\vec{v}_{i,k+\frac{1}{2}} = \vec{v}_{i,k-\frac{1}{2}} + (\Delta t)\vec{a}_{i,k,} \qquad k = 1, 2, 3, \ldots, \tag{14}$$

$$\vec{r}_{i,k+1} = \vec{r}_{i,k} + (\Delta t)\vec{v}_{i,k+\frac{1}{2}}, \qquad k = 0, 1, 2, 3 \ldots. \tag{15}$$

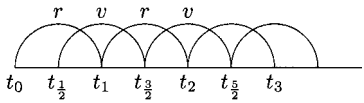

Fig. 1. The leapfrog updating scheme.

Note that (11) and (12) are two-point central difference formulas. The name leapfrog derives from the way position and velocity are defined at alternate, sequential time values. As shown in Fig. 1, r values are defined at the times $t_0, t_1, t_2, t_3, \ldots$ while the v values are defined at the times $t_{1/2}, t_{3/2}, t_{5/2}, t_{7/2}, \ldots$. The figure also symbolizes the children's game "leapfrog."

In all the examples to be discussed, the leapfrog formulas will be implemented on a Digital Alpha 275 or 533 (64-bit word) scientific PC and can be reproduced readily by anyone with such a personal computer. Examples which required supercomputer simulation will not be discussed in the present paper.

In our approach to N-body modelling, we will consider the following three cases:

- N small (say, $1 \leq N \leq 200$)
- N large (say, $200 \leq N \leq 10{,}000$)
- N very large (say, $10{,}000 < N < 10^{20}$)

2. N LARGE

2.1. A Cavity Problem

We begin with N large. The very first example will be discussed in great detail, the ideas and methodology of which extend directly to other examples.

Let us first construct a regular triangular grid of edge length 3.06 Å and with altitude 2.65 Å. We determine 4235 grid points in the XY plane as follows:

$$
\begin{array}{lll}
x(1) = -91.8, & y(1) = 0, & \\
x(i) = x(i-1) + 3.06, & y(i) = 0, & i = 2, 61, \\
x(62) = -90.27, & y(62) = 2.65 & \\
x(i) = x(i-1) + 3.06, & y(i) = 2.65, & i = 63, 121, \\
x(i) = x(i-121), & y(i) = y(i-121) + 5.30, & i = 122, 4235.
\end{array}
$$

At each point $(x(i), y(i))$ we set a water vapor molecule P_i, $i = 1, 4235$. This array is shown in Fig. 2(a). To complete the initial data, recall that in two dimensions the rms velocity v for a water vapor molecule at 150°C is $v = 6.23$ Å/ps. Each molecule is now assigned this speed in either the X or Y direction, determined at random, with its sign also determined at random.

Now, in two dimensions consider the square of side 183.6 Å, shown in Fig. 2(b). The interior is called the cavity *or* the basin of the square. This basin encloses the molecular fluid shown in Fig. 2(a). The four sides are called the walls.

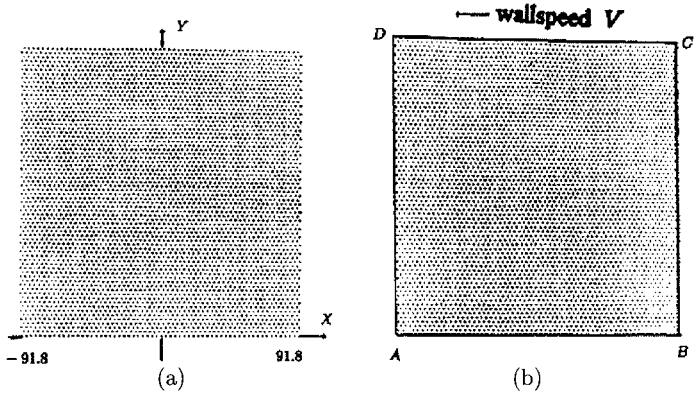

Fig. 2. (a) Array of water vapor molecules. (b) The same, but shown contained in a rigid-wall cavity in which the top wall, CD, is allowed to slide in the x direction at a velocity V.

The top wall, alone, CD, is allowed to move. It moves in the X direction at a constant speed V, called the wallspeed. Also it is allowed an extended length so that the molecular fluid is always completely enclosed by four walls. Then the cavity problem is to describe the gross motion of the fluid for various choices of V, which will be given in Å/ps (for laboratory studies of the cavity problem, see the treadmill apparatus of Freitas *et al*., 1985).

2.2. Computational Considerations

In all of our examples, the following computational considerations are implemented.

For time step Δt (ps), and $t_k = k\Delta t$, $k = 0, 1, 2, \ldots$, two problems must be considered relative to the computations. The first problem is to prescribe a protocol when, computationally, a molecule has crossed a wall into the exterior of the cavity. For each of the lower three walls, we will proceed as follows (no-slip condition). The position will be reflected back symmetrically, relative to the wall, into the interior of the basin, the velocity component tangent to the wall will be set to zero and the velocity component perpendicular to the wall will be multiplied by -1. If the molecule has crossed the moving wall, then its position will be reflected back symmetrically, its Y component of velocity will be multiplied by -1, and its X component of velocity will be increased by the wallspeed V.

The second problem derives from the fact that an instantaneous velocity field for molecular motion is Brownian. To better interpret gross fluid motion, we will introduce average velocities as follows. For J a positive integer, let particle P_i be at $(x(i, k), y(i, k))$ at t_k and at $(x(i, k - J), y(i, k - J))$ at t_{k-J}. Then the average

velocity $\vec{v}_{i,k,J}$ of P_i at t_k is defined by

$$\vec{v}_{i,k,J} = \left(\frac{x(i,k) - x(i,k-J)}{J\Delta t}, \frac{y(i,k) - y(i,k-J)}{J\Delta t} \right). \tag{16}$$

In the examples to be described, we will discuss results for various values of J.

Observe also that the connection between the wall speed V and the Reynolds number Re is given by Pan and Acrivos (1967).

$$\mathrm{Re} = |V|B/\nu, \tag{17}$$

in which B is the span, that is, the length CD in Fig. 2(a), and ν is the average kinematic viscocity of water. Thus, for example, for $V = -24$ Å/ps, $B = 183.6$ Å and, at 100°C (Streeter, 1962), $\nu = 30$ Å^2/ps, then (9) yields Re $= 147$.

2.3. Primary Vortex Generation

Consider first the parameter choices $V = -24$ Å/ps, $J = 20{,}000$, $\Delta t = 0.0001$ ps. Figure 3 shows the development of a primary vortex at the respective times $t = 4, 8, 14, 20$. An area of compression which precedes and drives the vortical motion is evident at $t = 4.0$. Other values of J which were studied were

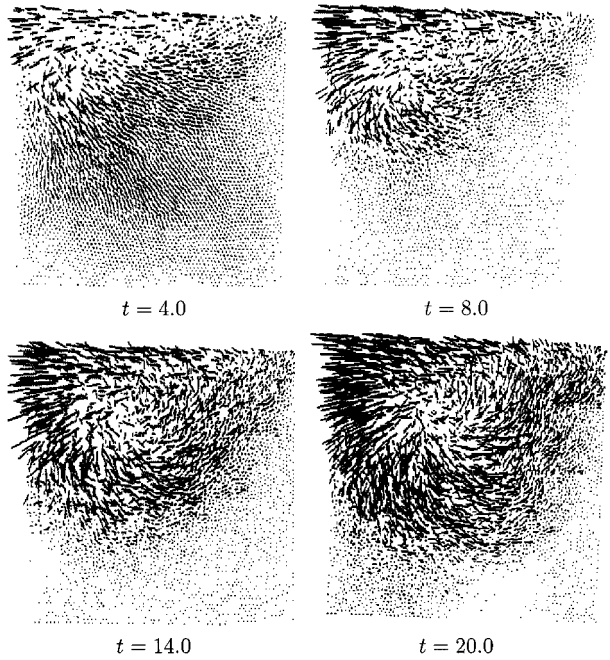

Fig. 3. Primary vortex generation. Wallspeed $= -24$, $J = 20,000$.

16,000, 12,000, 9000, and 6000, each of which yielded results similar to those of Fig. 3. Note that these results agree qualitatively with experimental results for cavity flow in the large (Freitas *et al.*, 1985).

Results similar to those in Fig. 3, but with larger primary vortices were obtained with $V = -40$, -130, and -600.

2.4. Turbulent Flow Generation

Turbulence is the most common yet least understood type of fluid flow. Turbulent flows have two well-defined characteristics:

- Many small vortices appear and disappear quickly (Kolmogorov, 1964), and
- A strong current develops across the usual primary direction (Schlichting, 1960).

Though mathematical fluid dynamicists are aware that the Navier–Stokes equations are not the equations of turbulent flow, engineers continue to generate "turbulent" flows using the Navier–Stokes equations with high Reynolds number (Ladyzhenskaya, 1969). It should also be observed that formulas of statistical mechanics are not applicable to turbulent flow (Batchelor, 1959; Bernard, 1998).

The discussion in section 2.3 for primary vortex generation now leads to the following approach to generating turbulent flows. For a sufficiently large magnitude of the wallspeed V, let us show that turbulence results when, for given Δt, a stable calculation results but no J exists which yields a primary vortex.

Let us then set $V = -3000$, $\Delta t = 2.5 \cdot 10^{-6}$. The motion was simulated to $t = 0.8$. Typical results are shown in Fig. 4 for $J = 80{,}000$, 60,000, 40,000, 20,000. None of these figures show a primary vortex because a strong current has developed across the primary vortex direction. Figure 5 shows an enlargement of the second frame of Fig. 4 in the range $45 \le x \le 91.8$, $10 \le y \le 100$, and reveals this crosscurrent clearly.

To support the contention that Fig. 4 represents fully turbulent flow, we now define the concept of a small vortex. For $3 \le M \le 6$, we define a small vortex as a flow in which M molecules nearest to an $(M+1)$st molecule rotate either clockwise or counterclockwise about the $(M+1)$st molecule and, in addition, the $(M+1)$st molecule lies interior to a simple polygon determined by the given M molecules. With this definition, Fig. 6(a) shows, for example, that the flow in the second frame in Fig. 4 has 185 small vortices at $t = 0.8$, while Fig. 6(b) shows that only 0.2 p before, that is, at $t = 0.6$, the resulting flow has 182 small vortices which are completely different from those in Fig. 6(a).

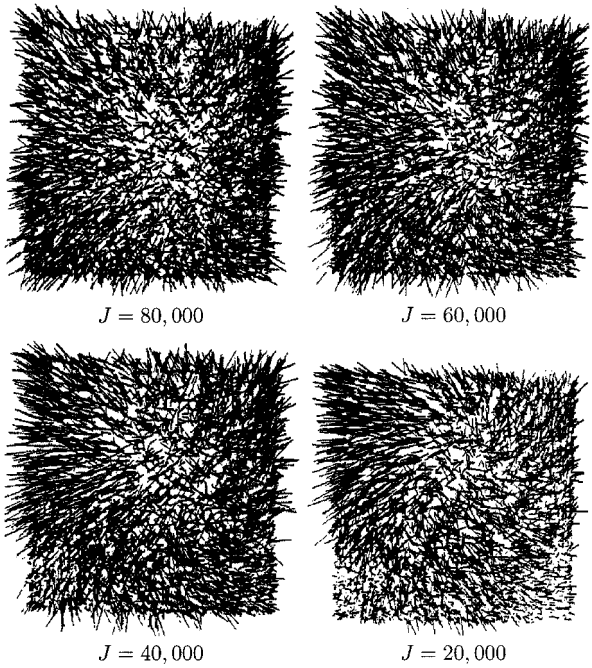

Fig. 4. Turbulent flow generation. Wallspeed $= -3000$, $t = 0.8$.

2.5. Primary Vortices and Turbulence for Air

Results entirely analogous to those for water vapor were obtained for the cavity problem for air. But in this case a new problem had to be resolved first. It is rather interesting that even though air is heterogeneous and consists of a variety of atoms and molecules, experimental Lennard–Jones potentials are readily available

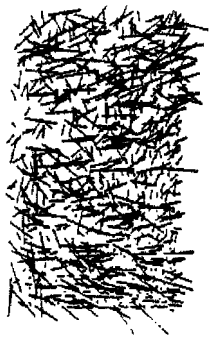

Fig. 5. Blowup of a right section of the second frame of Fig. 4.

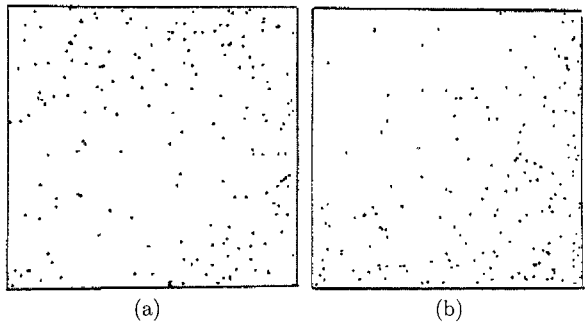

Fig. 6. (a) 185 small vortices at $t = 0.8$. (b) 182 small vortices at $t = 0.6$.

only for homogeneous air (Hirchfelder *et al.*, 1969). One such potential is

$$\phi(r_{ij}) = 5.36 \cdot 10^{-14} \left[\frac{3.617^{12}}{r_{ij}^{12}} - \frac{3.617^{6}}{r_{ij}^{6}} \right] \text{erg}.$$

Before one could proceed to dynamical considerations, it is necessary to characterize carefully the hypothetical air molecule to be used. We assume that the air to be used is nondilute and dry. Dry air consists primarily of 78% N_2, 21% O_2, and 1% Ar, whose respective masses are

$$m(\mathrm{N}_2) = 28 \cdot 1.660 \cdot 10^{-24} gr,$$
$$m(\mathrm{O}_2) = 32 \cdot 1.660 \cdot 10^{-24} gr,$$
$$m(\mathrm{Ar}) = 40 \cdot 1.660 \cdot 10^{-24} gr.$$

We now characterize an "air" molecule A as consisting of proportionate amounts of N_2, O_2, and Ar and having mass

$$m(A) = [0.78 \cdot 28 + 0.21 \cdot 32 + 0.01 \cdot 40] \cdot 1.660 \cdot 10^{-24} = 4.807 \cdot 10^{-23} gr.$$

With this hypothetical air molecule, the computations proceeded as for water vapor.

For the parameter choice $V = -40$, the resulting primary vortex at $t = 10.2$ is slightly larger than the corresponding one obtained for water vapor with $V = -40$ at $t = 10.2$. Indeed, the average speed for water vapor was 7.52 Å/ps while the average speed for air is 9.02 Å/ps, even though the initial velocity for water vapor was larger than that for air. For the parameter choice $V = -3000$, the turbulent flow is entirely analogous to that for water vapor. The average speed of the air molecules is 362 Å/ps at $t = 0.6$, while that for water at the same time was 353 Å/ps.

3. N VERY LARGE

3.1. Particle Simulation

Because statistical mechanics formulas are not applicable to turbulent flow, we will use a simple route of reducing this case to the case N large. This will allow us to apply the numerical methodology of the previous section. We will do this by invoking the engineering lumped mass approach, that is, molecules will be aggregated into particles by using mass and energy conservation. The particles will then be studied dynamically by means of molecular-type formulas, that is, formulas which include both attraction and repulsion. However, it will now be essential to include gravity.

3.2. Particle Arrangement and Equations for Water Vapor

Consider first a 30- by -240cm rectangle and on it construct a regular triangular grid with 8479 points, shown in Fig. 7(a), by the recursion formulas

$$\begin{array}{lll} x(1) = -15.0, & y(1) = 0.0, & \\ x(i) = x(i-1) + 1.0, & y(i) = 0.0, & i = 2, 31, \\ x(32) = -14.5, & y(32) = 0.866, & \\ x(i) = x(i-1) + 1.0, & y(i) = 0.866, & i = 33, 61, \\ x(i) = x(i-61), & y(i) = y(i-61) + 1.732, & i = 62, 8479. \end{array}$$

The side of each triangle in the grid has length of 1 cm. At each grid point $(x(i), y(i))$ set a particle P_i, that is, an aggregate of molecules. Thus, the distance between any two immediate neighbors is unity. Since the initial particle positions are now

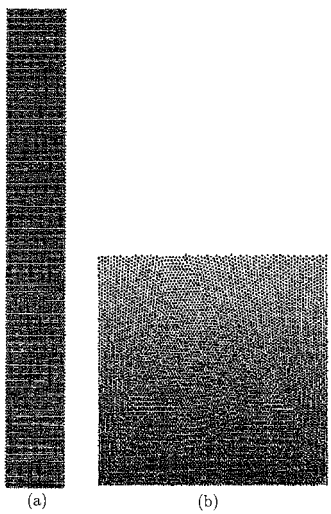

Fig. 7. (a) A 30 × 240 cm rectangle filled with 8479 particles arranged in a triangular array. (b) The bottom section of this rectangle, after most particles (namely, 7549) have settled near the bottom of the column.

known, we also assign each particle a small initial velocity of 0.00001 in the X or Y direction, determined at random, with its sign also determined at random.

The force between two distinct particles P_i and P_j which are R_{ij} cm apart will be taken to have magnitude F given by

$$F(R_{ij}) = -\frac{A}{R_{ij}^3} + \frac{B}{R_{ij}^5} \text{ (dynes)}. \tag{18}$$

The justification for this choice is as follows. First we wish to choose a formula which is qualitatively like (3) so that it too is composed of attraction and repulsion components. The choices of the exponents 3 and 5 guarantees further that the volatile motion between molecules with exponents 7 and 13 will not prevail for the more massive particles.

Thus, from (18),

$$\phi(R_{ij}) = -\frac{A}{2R_{ij}^2} + \frac{B}{4R_{ij}^4} \text{ (ergs)}. \tag{19}$$

Our first problem is to determine A and B. Assume that $F(1) = 0$, so that from (18),

$$-A + B = 0. \tag{20}$$

To determine a second equation, some relevant observations must be made first. Note that the number N of molecules which can be arranged in the rectangle using a regular triangular grid is

$$N = \frac{30}{3.06 \cdot 10^{-8}} \cdot \frac{240}{2.65 \cdot 10^{-8}} = 8.87 \cdot 10^{18}. \tag{21}$$

Also, note that since the mass of a water molecule is $30.103 \cdot 10^{-24}$ gr, the total mass M of the water molecules inside the 30×240 cm rectangle in Fig. 7(a) is

$$M = 2.67 \cdot 10^{-4} \text{ gr}. \tag{22}$$

Distributing this mass over the 8479 particles for conservation of total mass yields an individual particle mass (m) of

$$m = 3.15 \cdot 10^{-8} \text{ gr}. \tag{23}$$

From (2) and (21), the total potential energy E_{M} of the molecular configuration is, approximately,

$$E_{\mathrm{M}} = 3 \sum_{i=1}^{8.88 \cdot 10^{18}} 1.9646 \cdot 10^{-13} \left[\left(\frac{2.725}{3.06} \right)^{12} - \left(\frac{2.725}{3.06} \right)^{6} \right] = -1.3 \cdot 10^{6} \text{ erg}. \tag{24}$$

On the other hand, the total potential energy E_{p} of the particle configuration is, from (19), approximately,

$$E_{\mathrm{p}} = 3\sum_{i=1}^{8479}\left(-\frac{1}{2}A + \frac{1}{2}B\right) = 25,437\left(-\frac{1}{2}A + \frac{1}{2}B\right). \tag{25}$$

However, the kinetic energies of both the particle and molecular configurations are relatively negligible so that total energy is conserved by setting $E_{\mathrm{M}} = E_{\mathrm{p}}$. Thus the second equation for A and B is

$$25,437\left(-\frac{1}{2}A + \frac{1}{2}B\right) = -1.3 \cdot 10^6. \tag{26}$$

The solution of (20) and (26) is $A = B = 205$. Thus, (18) takes the particular form

$$F(R_{ij}) = 205\left(-\frac{1}{R_{ij}^3} + \frac{1}{R_{ij}^5}\right).$$

We assume next that two particles interact only within the local interaction distance $D = 1.3$ cm, which is the solution of the equation $\frac{dF}{dR_{ij}} = 0$.

The dynamical equation of motion for each particle P_i of the system is then given by

$$\frac{d^2\vec{R}_i}{dt^2} = -980\vec{\delta} + \frac{\alpha}{m}\sum_{\substack{j \\ j\neq i}} 205\left[\frac{1}{R_{ij}^5} - \frac{1}{R_{ij}^3}\right]\frac{\vec{R}_{ji}}{R_{ij}}; \qquad R_{ij} < D, \tag{27}$$

in which $\vec{\delta} = (0, 1)$, α is a parameter, and $i = 1, 8479$. The reason for the introduction of the parameter α is that particle interaction should be local relative to gravity, that is, gravity must dominate for R_{ij} less than, but close to, unity, which we assume to mean for $R_{ij} \geq 0.7$. However, this is the case if we choose $\alpha = m$, since, for $R_{ij} = 0.9, 0.8, 0.7, 0.6$, F takes the values 66, 225, 622, and 1687, respectively, the first three of which are less than 980. Thus, the dynamical equations for the particles are

$$\frac{d^2\vec{R}_i}{dt^2} = -980\vec{\delta} + \sum_{\substack{j \\ j\neq i}} 205\left[\frac{1}{R_{ij}^5} - \frac{1}{R_{ij}^3}\right]\frac{\vec{R}_{ji}}{R_{ij}}; \qquad R_{ij} < D. \tag{28}$$

It should be noted that other choices of α are also under study.

3.3. Particle Equilibrium

We now allow the 8479 particles in Fig. 7(a) to find their own equilibrium when interacting in accordance with (28). We choose $\Delta t = 0.0001$, and use the no-slip reflection protocol.

The initial motion of the system is almost one of free fall. So, for the first 20,000 time steps each velocity is damped by the factor of 0.2 every 20,000 time steps. For the next 20,000 time steps, each velocity is damped by the factor of 0.4 every 20,000 time steps. For the third 20000 time steps, each velocity is damped by the factor of 0.7 every 20,000 steps. For the final 20,000 steps the damping is removed. In this fashion, the particles are eased down into a stable configuration. Finally, to obtain a square set of particles, all particles with $y_i > 30$ are removed to yield the 7549 particle set shown in Fig. 7(b). The positions and velocities of these particles are used as the initial data for the cavity flow examples to be described next.

3.4. Examples

In the cavity examples which follow, we use the same protocol as was used for molecules in Sect. 2.2 with respect to wall reflection and averaging velocities.

Example 1. Consider now the cavity problem for the 7459 particles in Fig. 7(b). Let $V = -40$, $\Delta t = 0.00001$, and $J = 20{,}000$. Then Fig. 8 shows the development

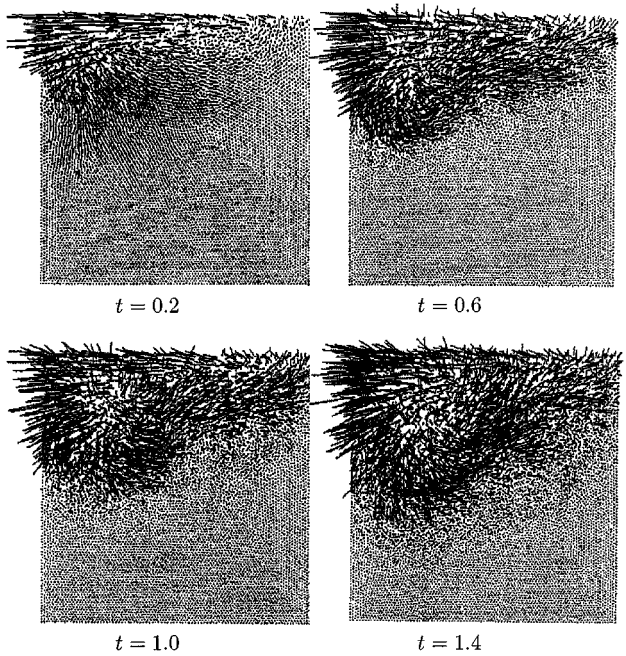

Fig. 8. Development of classical primary vortex.

of a classical primary vortex at the respective times $t = 0.2, 0.6, 1.0, 1.4$. Entirely similar results followed for $J = 14{,}000, 11{,}000, 9000$.

Results analogous to those just described were obtained also with $V = -100$, -250, -600, but the size of the primary vortex increased with the wall speed.

Example 2. To simulate turbulence, set $V = -3000$, $\Delta t = 5(10)^{-7}$, $J = 80{,}000$. Figure 9 shows the flow development at the respective times 0.04, 0.08, 0.12, 0.15. The first frame shows that the motion begins with a compression wave. The next two frames show that the ensuing particle repulsion is up and to the right in the usual primary vortex direction. The last frame shows the large crosscurrent over the usual primary vortex direction. Again, to support the contention that this last frame represents fully turbulent flow, we use the concept of a small vortex stated in Sect. 2.4. In searching for small vortices, attention was confined to within a circle of radius 1 cm around each particle. There resulted 355 small vortices which are shown in Fig. 10(a). Moreover, Fig. 10(b) shows the distribution of 349 small vortices at the time $t = 0.18$, so that, after only 0.03 s, this figure shows the rapid change throughout the cavity of the vortex distribution shown in Fig. 10(a).

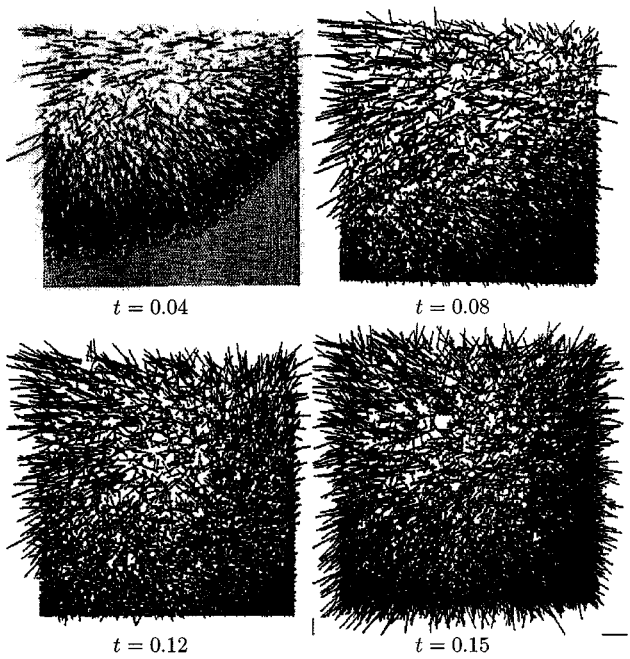

Fig. 9. Development of turbulent flow. $V = -3000$.

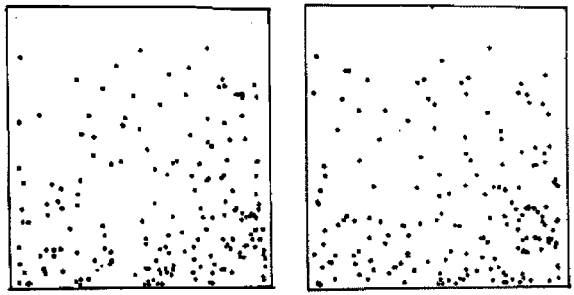

Fig. 10. (a) 355 small vortices at $t = 0.15$. (b) 349 small vortices at $t = 0.18$.

Entirely similar results for Fig. 9 followed with $J = 60{,}000, 40{,}000, 20{,}000$.

Other examples of particle models include the stress and crack development in a slotted copper plate (Greenspan, 1989) and approximation of the contact angle of adhesion of a sessile drop on a solid surface (Korlie, 1997).

4. MOLECULAR PARAMETERS UNAVAILABLE

4.1. Qualitative Models

Although quantitative models are always to be preferred, in many interesting cases the molecular parameters may not be known. For such cases, we often develop qualitative models. Such models do provide the researcher with several advantages, including

- the development of intuition,
- allowance for variation of parameters to determine which parameters are of most significance, and
- development of insights into the mechanisms of material behavior.

With this in mind, we examine next a qualitative model.

Example. (Soliton collision (Greenspan, 2001)). Figures 11 and 12 show, by means of a discrete string composed of 1001 particles, rather than by means of the KdV equation, the motion of two solitons and their passage through each other. This model is of value because it allows one to show the velocity fields of the particles during the complex collision, as demonstrated in Fig. 12.

Other qualitative models have simulated the biological self-reorganizatuion of separated tissue cells (Greenspan, 1997; Steinberg, 1963) the bounce of an elastic ball (Greenspan, 2000), and the generation of the unstable equilibrium position of an elastic snap through (Greenspan and Casulli, 1985).

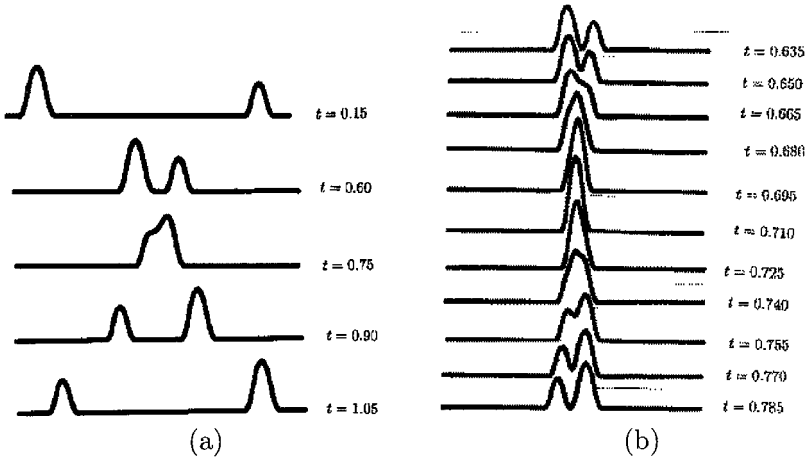

Fig. 11. Passage of two solitons through one another: (a) Overall view. (b) Higher time resolution around $t = 0.75$.

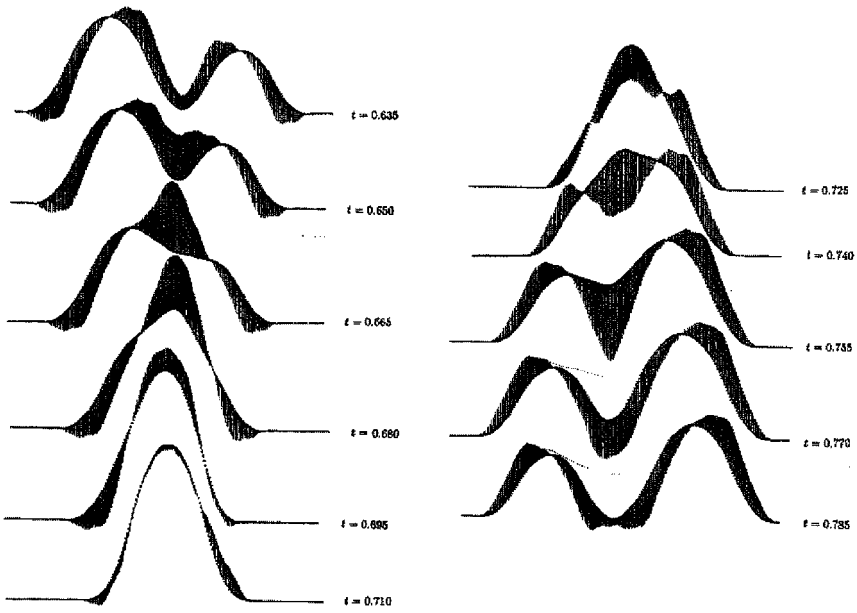

Fig. 12. Passage of two solitons through one another, showing both position and velocity.

5. *N* SMALL

Now, if N is small, we would do a very good job in solving the N-body problem. By this we mean that we would like not only to solve the problem with accuracy, but we would also like to preserve numerically any basic physical invariants of the system. To do this in detail, we concentrate on the 3-body problem, which is the prototype problem because it contains all the difficulties of the general N-body problem. The entire discussion extends in a natural way to the general problem.

For $i = 1, 2, 3$, let P_i of mass m_i be at $\vec{r}_i = (x_i, y_i, z_i)$ at time t. Let the positive distance between P_i and P_j, $i \neq j$, be $r_{ij} = r_{ji}$. Let $\phi = \phi_{ij} = \phi(r_{ij})$, given in ergs, be the potential for the pair P_i, P_j. Then the force on P_i due to P_j is

$$\vec{F}_i = -\frac{\partial \phi}{\partial r_{ij}} \frac{\vec{r}_i - \vec{r}_j}{r_{ij}},$$

and the Newtonian dynamical differential equations for the 3-body problem are

$$m_i \frac{d^2 \vec{r}_i}{dt^2} = -\frac{\partial \phi}{\partial r_{ij}} \frac{\vec{r}_i - \vec{r}_j}{r_{ij}} - \frac{\partial \phi}{\partial r_{ik}} \frac{\vec{r}_i - \vec{r}_k}{r_{ik}}, = 1, 2, 3, \tag{29}$$

where $i = 1$ implies $j = 2$, $k = 3$; $i = 2$ implies $j = 1$, $k = 3$; $i = 3$ implies $j = 1$, $k = 2$.

The following summary theorem incorporates several well-known results.

Theorem 5.1. *System (29) conserves energy, linear momentum, and angular momentum. It is also covariant under translation, rotation, and uniform relative motion of coordinate frames (Goldstine, 1980).*

To solve an initial value problem for (29) numerically, we will first rewrite it as the equivalent first-order system

$$\frac{d\vec{r}_i}{dt} = \vec{v}_i, \qquad i = 1, 2, 3, \tag{30}$$

$$m_i \frac{d\vec{v}_i}{dt} = -\frac{\partial \phi}{\partial r_{ij}} \frac{\vec{r}_i - \vec{r}_j}{r_{ij}} - \frac{\partial \phi}{\partial r_{ik}} \frac{\vec{r}_i - \vec{r}_k}{r_{ik}}, \quad i = 1, 2, 3. \tag{31}$$

Our numerical formulation now proceeds as follows. For $\Delta t > 0$, let $t_n = n(\Delta t)$, $n = 0, 1, 2, \ldots$. At time t_n, let P_i be at $\vec{r}_{i,n} = (x_{i,n}, y_{i,n}, z_{i,n})$ with velocity $\vec{v} = (v_{i,x,n}, v_{i,y,n}, v_{i,z,n})$. Denote the distances $\|P_1P_2\|$, $\|P_1P_3\|$, $\|P_2P_3\|$ by $r_{12,n}, r_{13,n}, r_{23,n}$, respectively. Differential Eqs. (30) and (31) are now approximated, respectively, by the difference equations

$$\frac{\vec{r}_{i,n+1} - \vec{r}_{i,n}}{\Delta t} = \frac{\vec{v}_{i,n+1} + \vec{v}_{i,n}}{2}, \tag{32}$$

$$m_i \frac{\vec{v}_{i,n+1} - \vec{v}_{i,n}}{\Delta t} = -\frac{\phi(r_{ij,n+1}) - \phi(r_{ij,n})}{r_{ij,n+1} - r_{ij,n}} \frac{\vec{r}_{i,n+1} + \vec{r}_{i,n} - \vec{r}_{j,n+1} - \vec{r}_{j,n}}{r_{ij,n+1} + r_{ij,n}}$$
$$-\frac{\phi(r_{ik,n+1}) - \phi(r_{ik,n})}{r_{ik,n+1} - r_{ik,n}} \frac{\vec{r}_{i,n+1} + \vec{r}_{i,n} - \vec{r}_{k,n+1} - \vec{r}_{k,n}}{r_{ik,n+1} + r_{ik,n}}. \tag{33}$$

Note that the force is approximated, not the potential. We take the very same potential as in continuum mechanics, the significance of which will be seen shortly. Consistency follows immediately as $\Delta t \to 0$.

System (32), (33) consists of 18 implicit equations for the unknowns

$$x_{i,n+1},\ y_{i,n+1},\ z_{i,n+1},\ v_{i,x,n+1},\ v_{i,y,n+1},\ v_{i,z,n+1}$$

in the 18 knowns

$$x_{i,n},\ y_{i,n},\ z_{i,n},\ v_{i,x,n},\ v_{i,y,n},\ v_{i,z,n}$$

and is solvable readily by Newton's method (Greenspan, 1997).

We now state for our numerical method the following theorem which is the difference analogue of Theorem 5.1.

Theorem 5.2. *The numerical method conserves exactly the same energy, linear momentum and angular momentum as does differential system (29), and does this independently of the time step Δt. In addition the difference equations are covariant under translation, rotation, and uniform relative motion of coordinate frames (Greenspan, 1997).*

Rather than give the proof of all parts of the theorem, let us show in complete detail the proof of conservation of energy to indicate the methodology used.

Proof: Define

$$W_N = \sum_{n=0}^{N-1} \sum_{i=1}^{3} m_i (\vec{r}_{i,n+1} - \vec{r}_{i,n}) \cdot \frac{(\vec{v}_{i,n+1} - \vec{v}_{i,n})}{\Delta t}. \tag{34}$$

Then, from (32).

$$W_N = \sum_{n=0}^{N-1} \sum_{i=1}^{3} m_i \frac{(\vec{r}_{i,n+1} - \vec{r}_{i,n})}{\Delta t} \cdot (\vec{v}_{i,n+1} - \vec{v}_{i,n}).$$
$$= \sum_{n=0}^{N-1} \sum_{i=1}^{3} m_i \frac{(\vec{v}_{i,n+1} + \vec{v}_{i,n})}{2} \cdot (\vec{v}_{i,n+1} - \vec{v}_{i,n})$$

$$
\begin{aligned}
&= \sum_{n=0}^{N-1} \sum_{i=1}^{3} m_i \left(\frac{v_{i,n+1}^2}{2} - \frac{v_{i,n}^2}{2} \right) \\
&= \sum_{i=1}^{3} \frac{1}{2} m_i \left[\left(v_{i,1}^2 - v_{i,0}^2 \right) + \left(v_{i,2}^2 - v_{i,1}^2 \right) + \left(v_{i,3}^2 - v_{i,2}^2 \right) + \cdots \right. \\
&\quad \left. + \left(v_{i,N}^2 - v_{i,N-1}^2 \right) \right] \\
&= \frac{1}{2} m_1 v_{1,N}^2 + \frac{1}{2} m_2 v_{2,N}^2 + \frac{1}{2} m_3 v_{3,N}^2 - \frac{1}{2} m_1 v_{1,0}^2 - \frac{1}{2} m_2 v_{2,0}^2 - \frac{1}{2} m_3 v_{3,0}^2 \\
&= K_N - K_0
\end{aligned}
$$

Next, observing first that $\vec{r}_i - \vec{r}_j = \vec{r}_{ji}$, and then substituting (33) into (34) yields with simple algebraic manipulation that

$$
\begin{aligned}
W_N &= \sum_{n=0}^{N-1} (-\phi_{12,n+1} - \phi_{13,n+1} - \phi_{23,n+1} + \phi_{12,n} + \phi_{13,n} + \phi_{23,n}) \\
&= -\phi_{12,N} - \phi_{13,N} - \phi_{23,N} + \phi_{12,0} + \phi_{13,0} + \phi_{23,0} \\
&= -\phi_N + \phi_0.
\end{aligned}
$$

Hence,

$$K_N - K_0 = -\phi_N + \phi_0$$

or

$$K_N + \phi_N = K_0 + \phi_0, \qquad N = 0, 1, 2, 3, \ldots$$

Moreover, since K_0 and ϕ_0 depend only on $\vec{r}_{i,0}$ and $\vec{v}_{i,0}$, it follows that $K_0 + \phi_0$ is the same in both the continuous and the discrete cases, so that the energy conserved is exactly that of the continuous system. Note also that the proof was independent of Δt. □

Example. Motion of a discrete dodecahedral top on a smooth surface (Greenspan, 1997).

Rigid body motion is of fundamental interest in mathematics, science, and engineering. We will consider a discrete dodecahedral body and simulate its motion when it spins like a top. The approach will not require the use of special coordinates, Cayley–Klein parameters, tensors, dyadics, or related concepts (Goldstine, 1980). All that is required is the conservative numerical methodology developed above.

Consider, now, in XYZ space as shown in Fig. 13(a), a dodecahedron P_1–P_8. For the present, let the distances between the vertices be given as follows:

$$\|P_1P_j\| = \|P_jP_8\| = 2\,\text{cm}, \qquad j = 2, \ldots, 7,$$
$$\|P_2P_3\| = \|P_3P_4\| = \|P_4P_5\| = \|P_5P_6\| = \|P_6P_7\| = \|P_7P_8\| = 1\,\text{cm},$$
$$\|P_2P_5\| = \|P_3P_6\| = \|P_4P_7\| = 2\,\text{cm}.$$

The vertices P_2–P_7 are taken to be vertices of a regular, plane hexagon with edge length 1 cm. The hexagon is located in the plane $z = \sqrt{3}$ and the vertex coordinates are

$$P_2(0,\,1,\,\sqrt{3}), \quad P_3\left(\tfrac{1}{2}\sqrt{3},\,\tfrac{1}{2},\,\sqrt{3}\right), \quad P_4\left(\tfrac{1}{2}\sqrt{3},\,-\tfrac{1}{2},\,\sqrt{3}\right),$$
$$P_5(0,\,-1,\,\sqrt{3}), \quad P_6\left(-\tfrac{1}{2}\sqrt{3},\,-\tfrac{1}{2},\,\sqrt{3}\right), \quad P_7\left(-\tfrac{1}{2}\sqrt{3},\,\tfrac{1}{2},\,\sqrt{3}\right).$$

The geometric center of the hexagon is the point $Q(0,\,0,\,\sqrt{3})$. The point P_8, located on the line through P_1Q, is at $P_8(0,\,0,\,2\sqrt{3})$.

To set the top in rotation, the initial velocities of P_2–P_7 are chosen to be, as shown in Fig. 13(b), respectively,

$$\vec{v}_2 = (v,\,0,\,0), \quad \vec{v}_3 = \left(\tfrac{1}{2}v,\,-\tfrac{1}{2}v\sqrt{3},\,0\right), \quad \vec{v}_4 = \left(-\tfrac{1}{2}v,\,-\tfrac{1}{2}v\sqrt{3},\,0\right),$$
$$\vec{v}_5 = (-v,\,0,\,0), \quad \vec{v}_6 = \left(-\tfrac{1}{2}v,\,\tfrac{1}{2}v\sqrt{3},\,0\right), \quad \vec{v}_7 = \left(\tfrac{1}{2}v,\,\tfrac{1}{2}v\sqrt{3},\,0\right),$$

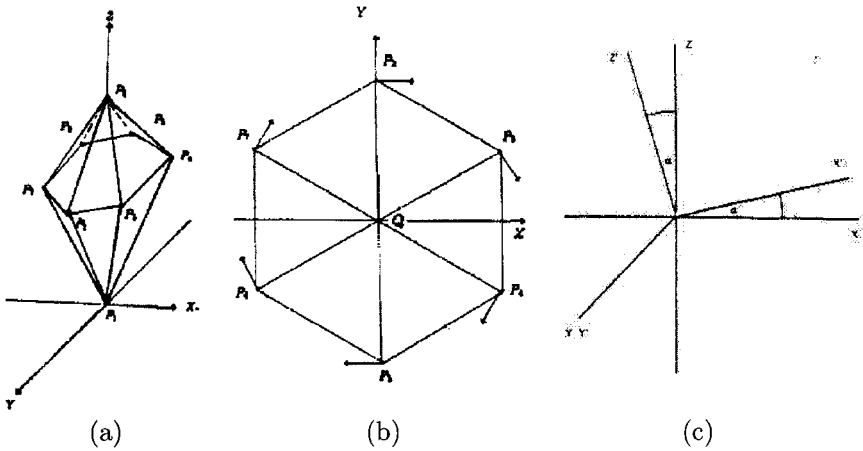

Fig. 13. (a) The dodecahedron. (b) Planar hexagon and initial velocities. (c) The rotation of the XZ plane.

so that the velocity of each particle is perpendicular to the line joining it to Q. The points P_1 and P_8 are given zero initial velocities.

Next, we want to tilt the top and this is done by rotating the XZ plane through an angle α, as shown in Fig. 13(c). Thus, the initial positions (x_i', y_i', z_i') and initial velocities $(v_{i,x'}, v_{i,y'}, v_{i,z'})$ of P_1–P_8 are determined finally by

$$x_i' = x_i \cos\alpha + z_i \sin\alpha, \quad y_i' = y_i, \quad z_i' = -x_i \sin\alpha + z_i \cos\alpha,$$

$$v_{ix'} = v_{ix} \cos\alpha + v_{iz} \sin\alpha, \quad v_{iy'} = v_{iy}, \quad v_{iz'} = -v_{ix} \sin\alpha + v_{iz'} \cos\alpha.$$

Thus, once the parameters v and α are given, all initial data for a tilted, rotating dodecahedral top are determined, and the resulting 8-body problem will be solved with energy, linear momentum and angular momentum conserved. Note also that because the top is rigid, a description of the motions of P_1 and Q suffice to determine the motion of the entire top.

The force formulas and the subtleties of their application are detailed in Greenspan (1997).

5.1. Examples

Example 1. Let $\alpha = 15^\circ$, $v = 400$. The conservative numerical formulas were then run for 200,000,000 time steps with a printout every 100,000 steps. The resulting motion of P_1 for the first cycle is shown in Fig. 14(a), which contains 1086 points, on the region $x \in [-0.32, 3.1]$, $y \in [-1.71, 1.71]$. and in the enlarged version in Fig. 14(b) on the region $x \in [-0.196, 0.916]$, $y \in [-0.4678, 0.4678]$.

The motion is characterized by a circular, cycloid-type trajectory around the central point (0.4483,0) in the XY plane. The point (x^*, y^*, z^*) is always on the line (0.4483, 0, z) with z^* varying in the range [1.668, 1.673].

Example 1 is typical of a variety of others studied in which the parameters v and α were varied. Let us then examine a difficult problem in which certain masses are not all the same.

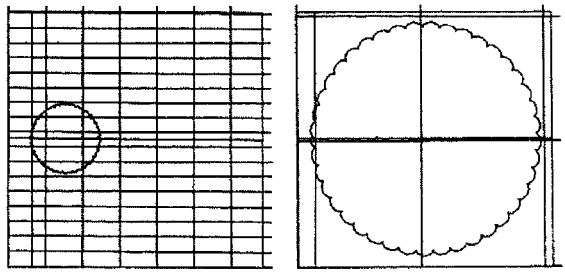

Fig. 14. (a) First cycle of a cycloid-like trajectory, shown enlarged in (b).

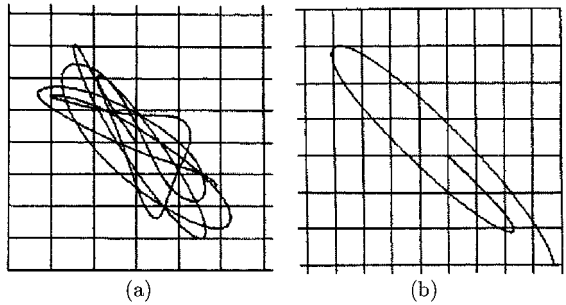

Fig. 15. (a) Looping trajectory, with initial part shown enlarged in (b).

Example 2. As in Example 1, let $\alpha = 15^\circ$, $v = 400$, but set $m_2 = 2$, $m_4 = 4$. The conservative numerical formulas were then run for 100,000 time steps with a printout every 20 steps. Figure 15(a) shows the trajectory of P_1, for the first 4000 points, in the region $x \in [-0.015, 0.015]$, $y \in [-0.02, 0.02]$. Figure 15(b) shows an enlarged version of the motion of the first 1000 points in the region $x \in [-0.008, 0.1]$, $y \in [-0.02, 0.015]$.

Both figures reveal large looping motions for P_1. The graphics procedure available was insufficient to determine whether or not small cusps were part of the trajectory. Figure 16 shows the erratic motion over the full 5000 points of Q in the narrow three-dimensional range $x^* \in [0.444, 0.452]$, $y^* \in [-0.008, 0.008]$, $z^* \in [1.670, 1.676]$.

Another application of conservative methodology has been made to Calogero and Toda Hamiltonian systems (Greenspan, 1990).

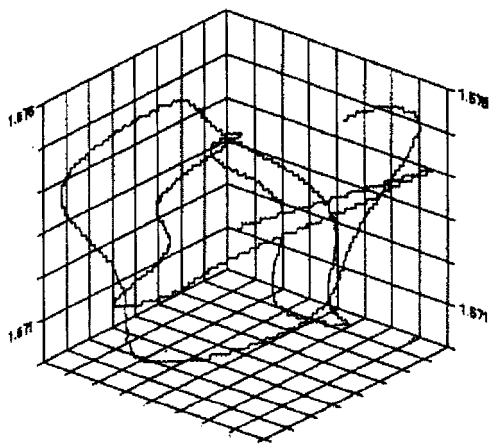

Fig. 16. Looping trajectory in three dimensions.

6. THE 1-BODY PROBLEM (GREENSPAN, 1997)

Interestingly enough, there exist some very important 1-body problems, and these occur in *special relativity*. Let us then turn to a basic dynamical problem in special relativity and begin by discussing the very few concepts which will be required for the development.

In special relativity one takes into account the time required for light to travel from a phenomenon being observed to the eye of the observer. Consider, then, two reference frames: a LAB frame with Euclidean coordinates X, Y, Z and a ROCKET frame with Euclidean coordinates X',Y',Z', which coincide initially. In the frames one positions observers O and O' at their respective origins. At some intial time the observers have synchronized clocks. Assume the rocket frame is in motion in the X direction with speed u relative to the lab frame. An event P, like an exploding star, is observed by both O and O'. O records P as happening at (x, y, z) at time t, while O' records P as happening at (x', y', z') at time t'. Taking into account the time for light to travel to the eyes of the observers, these variables are related by the Lorentz transformation:

$$x' = \frac{c(x-ut)}{(c^2-u^2)^{\frac{1}{2}}}, \quad y' = y \quad z' = z \quad t' = \frac{(c^2t-ux)}{(c^2-u^2)^{1/2}}, \tag{35}$$

in which c is the speed of light.

For *covariance* relative to the Lorentz transformation, Einstein showed that for the motion of a particle P of rest mass m_0

$$F = \frac{d}{dt}(mv), \qquad m = \frac{cm_0}{(c^2-v^2)^{1/2}} \qquad \text{(LAB)}, \tag{36}$$

maps under the Lorentz transformation into

$$F' = \frac{d}{dt'}(m'v'), \qquad m' = \frac{cm_0}{(c^2-v'^2)^{\frac{1}{2}}} \qquad \text{(ROCKET)}, \tag{37}$$

that is, the laws of motion are the same in both the lab frame and the rocket frame.

Now, in the lab frame the equation of so simple an oscillator as the harmonic oscillator has a nonlinear equation of the form (Greenspan, 1997)

$$\ddot{x} + (1-\dot{x}^2)^{3/2}x = 0,$$

coupled with initial conditions

$$x(0) = \alpha, \qquad \dot{x}(0) = \beta,$$

which requires numerical methodology.

Thus, one now must insert identical computers into the LAB and ROCKET frames and ask how the observers can solve the problem of harmonic motion numerically so that the physics of special relativity is preserved, that is, so that the

numerical results of the observers are related by the Lorentz transformation. This is accomplished as follows.

For $\Delta t > 0$, let $t_n = n\Delta t$, $n = 0, 1, 2, 3, \ldots$. Let t'_n correspond to t_n by the Lorentz transformation. At t_n let P be at (x_n, y_n, z_n) in the LAB and at (x'_n, y'_n, z'_n) in the ROCKET. These are also related by the Lorentz transformation. Define

$$v_n = \frac{\Delta x_n}{\Delta t_n}, \qquad a_n = \frac{\Delta v_n}{\Delta t_n} \qquad \text{(LAB)}, \tag{38}$$

$$v'_n = \frac{\Delta x'_n}{\Delta t'_n}, \qquad a'_n = \frac{\Delta v'_n}{\Delta t'_n} \qquad \text{(ROCKET)}. \tag{39}$$

Then the following theorems are valid (Greenspan, 1997):

Theorem 6.1. *(Covariance). Under the Lorentz transformation*

$$F_n = \frac{c^2 m_n}{\left[\left(c^2 - v_n^2\right)\left(c^2 - v_{n+1}^2\right)\right]^{\frac{1}{2}}} \frac{\Delta v_n}{\Delta t_n}, \qquad m_n = \frac{cm_0}{\left(c^2 - v_n^2\right)^{1/2}} \tag{40}$$

transforms into

$$F'_n = \frac{c^2 m'_n}{\left[\left(c^2 - v_n'^2\right)\left(c^2 - v_{n+1}'^2\right)\right]^{\frac{1}{2}}} \frac{\Delta v'_n}{\Delta t'_n}, \qquad m'_n = \frac{cm_0}{\left(c^2 - v_n'^2\right)^{1/2}}. \tag{41}$$

Moreover, (40) and (41) converge to the Einstein equations as the time steps converge to zero, that is, consistency is valid.

Interestingly enough, (38)–(41) can be solved explicitly to yield

$$x_{k+1} = x_k + (\Delta t_k) v_k, \tag{42}$$

$$v_{k+1} = \frac{v_k + (\Delta t_k)(1 - (v_k)^2) F_k \sqrt{1 - (v_k)^2 + (\Delta t_k)^2 (1 - (v_k)^2)^2 (F_k)^2}}{1 + (\Delta t_k)^2 (1 - (v_k)^2)^2 (F_k)^2}, \tag{43}$$

$$x'_{k+1} = x'_k + (\Delta t'_k) v'_k, \tag{44}$$

$$v'_{k+1} = \frac{v'_k + (\Delta t'_k)(1 - (v'_k)^2) F'_k \sqrt{1 - (v'_k)^2 + (\Delta t'_k)^2 (1 - (v'_k)^2)^2 (F'_k)^2}}{1 + (\Delta t'_k)^2 (1 - (v'_k)^2)^2 (F'_k)^2} \tag{45}$$

from which the computations are readily done.

Let us assume now that $x(0) = x_0 = 0$. Then Fig. 17 shows how the amplitude of the relativistic harmonic oscillator deviates from that of the Newtonian harmonic oscillator with increasing v_0.

Finally we have a major theorem (Greenspan, 1997):

Theorem 6.2. *Using (38) and (40) numerically in the LAB, and using (39) and (41) numerically in the ROCKET results in numerical results which are related by the Lorentz transformation.*

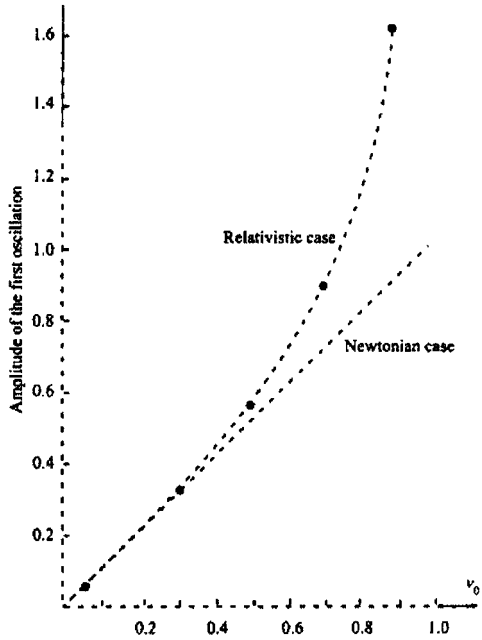

Fig. 17. Amplitude of a relativistic harmonic oscillator as a function of v_0.

7. SUMMARY

In this paper we have directed attention to new discrete models of solids, liquids, and gases. Our approach is based on the atomic and molecular structure of matter. It is practical because of the availability of modern digital computers, and because quantum mechanical principles, like uncertainty, which makes electron positions fuzzy within an atom, place few important restrictions on how a stable atom can be held in place. Indeed, a stable atom, on the whole, has a comparatively definite position set by its comparatively massive nucleus (Feynman, 1959). This observation was supported and clarified by Feynman (1959) in a lecture to the American Physical Society in which he also said, (a) "The principles of physics, as far as I can see, do not speak against the possibility of maneuvering things atom by atom," and (b) "The problems of chemistry and biology can be greatly helped if our ability to see what we are doing, and to do things on an atomic level, is relatively developed—a development which I think cannot be avoided." Feynman then discussed specific areas of development and application, and thereby initiated a new branch of physics, called nanophysics, and a new branch of technology, called nanotechnology, which are both in energetic states of development.

In our models we have replaced continuous structures and small systems of partial differential equations by discrete structures and large systems of ordinary differential equations. The advantage in doing so is that it then becomes possible to study phenomena which are not consequences of continuum equations. This is the case of turbulent fluid flow which we have explored in sections 2.4 and 3.4. The basic mathematical problem for all our studies is the N-body problem described in complete generality in section 1.1

REFERENCES

Batchelor, G. K. (1959). *The Theory of Homogeneous Turbulence*, Cambridge University Press, Cambridge.

Bernard, P. S. (1998). Transition and turbulence. Basic physics. In *The Handbook of Fluid Dynamics*, Johnson, R. W. ed., CRC Press, Boca Raton, FL, p. 13–5.

Feynman, R. P. (1959). There's plenty of room at the bottom. Invited Lecture, Ann. Meet. APS, Cal. Inst. Tech., Pasadena. www.zyvex.com/nanotech/feynman.html.

Feynman, R. P., Leighton, R. B., and Sands, M. (1963). *The Feynman Lectures on Physics*, Vol. I, Addison-Wesley, Reading, MA.

Freitas, C. J., Street, R. L., Findikakis, A. N., and Koseff, J. R. (1985). Numerical simulation of thre dimensional flow in a cavity. *International Journal for Numerical Methods in Fluids* **5**, 561–575.

Goldstine, H. (1980). *Classical Mechanics*, 2nd edn., Addison-Wesley, Reading, MA.

Greenspan, D. and Casulli, V. (1985). Particle modelling of an elastic arch, *Applied Mathematical Modelling* **9**, 215–219.

Greenspan, D. (1989). Supercomputer simulation of cracks and fractures by quasimolecular dynamics. *International Journal of Physics and Chemistry of Solids* **50**, 1245–1249.

Greenspan, D. (1990). Conservative difference formulation of Calogero and Toda Hamiltonian systems, *Computers and Mathematics with Application* **19**, 91–95.

Greenspan, D. (1997). *Particle Modeling*, Birkhauser, Boston.

Greenspan, D. (2000). Particle simulation in contact mechanics of a bouncing elastic ball, *Mathematical and Computer Modelling* **32**, 803–812.

Greenspan, D. (2001). Discrete string solitons (Tech. Report 343), Departmen of Mathematics, UTA, Arlington, TX, May.

Hirschfelder, J. O., Curtiss, C. F., and Bird, R. B. (1967). *Molecular Theory of Gases and Liuids*, Wiley, New York.

Kolmogorov, A. N. (1964). Toward a more precise notion of the structure of the local turbulence in a viscous fluid at elevated Reynolds number. In *The Mechanics of Turbulence*, A. Favre, ed., Gordon and Breach, New York, pp. 447–458.

Korlie, M. S. (1997). Particle modeling of liquid drop formation on a solid surface in 3-D, *Computers and Mathematics with Applications* **33**, 97–114.

Ladyzhenskaya, O. A. (1969). *The Mathematical Theory of Viscous Incompressible Flow*, 2nd ed., Gordon and Breach, New York.

Pan, F. and Acrivos, A. (1967). *Steady flows in a rectangular cavity*. *J. Fluid Mech.*, **28**, 643–655.

Schlichting, H. (1960). *Boundary Layer Theory*, 4th ed., McGraw-Hill, New York.

Steinberg, M. S. (1963). Reconstruction of tissues by disassociated cells, *Science* **141**, 401–403.

Streeter, V. L. (1962). *Fluid Mechanics*, 3rd edn., McGraw-Hill, New York.